2015 IEEE International Conference on Robotics and Automation (ICRA)
Washington State Convention Center
Seattle, Washington, May 26-30, 2015

Injected 3D Electrical Traces in Additive Manufactured Parts with Low Melting Temperature Metals

John P. Swensen, *Member, IEEE*, Lael U. Odhner, *Member, IEEE*, Brandon Araki, and Aaron M. Dollar, *Senior Member, IEEE*

***Abstract*— While techniques exist for the rapid prototyping of mechanical and electrical components separately, this paper describes a method where commercial Additive Manufacturing (AM) techniques can be used to concurrently construct the mechanical structure and electronic circuits in a robotic or mechatronic system. The technique involves printing hollow channels within parts that are then filled with a low melting point liquid metal alloy that solidifies upon cooling to form electrical traces. This method is compatible with most conventional fused deposition modeling and stereolithography machines, and requires no modification to an existing printer, though the technique could easily be incorporated into multi-material machines. Three primary considerations are explored using the a commercial fused deposition manufacturing (FDM) process as a testbed: material and manufacturing process parameters, simplified injection fluid mechanics, and automatic part generation using standard printed circuit board software tools. As demonstration of the ability to embed circuit in RP parts, a differential-drive robot is printed, populated with discrete electronic components, and injected to create a fully functional robot.**

I. Introduction

Rapid fabrication processes such as stereolithography (SLA) and fused deposition modeling (FDM) have had a profound impact in many domains, including the production of robotic and mechatronic systems. While this impact has been, to date, primarily within the research domain, the build quality and robustness of systems produced using additive manufacturing (AM) techniques is beginning to allow for commercial-grade systems to be produced. When best-practice design rules are followed, (e.g. [1], [2]), high-quality hardware that might take weeks to fabricate by conventional CNC machining processes can be made in days or even hours at a fraction of the cost. This gives researchers an unprecedented ability to iteratively redesign robots based on experiments, and also enables the open publication of complete hardware designs in an easily reproducible form [3]–[5].

Traditionally, electronics for robotics and mechatronics have been done using standard prototyping boards or commercially manufactured printed circuit boards (PCB).

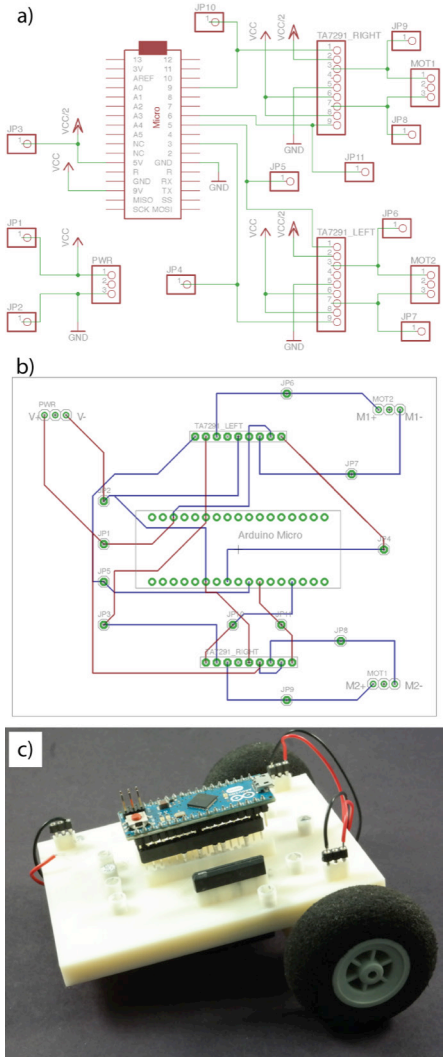

Figure 1. The process of creating circuits by designing hollow channels in 3D printed parts and injecting with low melting point metals to create complete electrical traces: (a) a schematic capture of a simple differential-drive robot, (b) a corresponding PCB layout, and (c) the populated circuit board with motors, wheels, and battery power.

And while there are well-developed processes and design tools for the generation of circuits using these traditional methods, the integration with hardware is almost always done through mounting of the circuit board to the robot hardware and associated cabling during robot assembly. A next frontier in rapid fabrication in these domains is electronic integration. Although processes such as Shape Deposition Manufacturing (SDM) have been used to create robots with embedded sensors and actuators [6], [7], techniques for rapid fabrication

Research supported by DARPA grant no. D13AP00056.

John P. Swensen and Aaron M. Dollar are with Yale University, New
John P. Swensen and Aaron M. Dollar are with Yale University, New Haven, CT 06511. (Corresponding author: John P. Swensen; e-mail: john.swensen@yale.edu).

Lael U. Odhner is with RightHand Robotics, Cambridge, MA. (e-mail: lael@righthandrobotics.com).

Brandon Araki is with the Massachusetts Institute of Technology, Cambridge, MA 02139. (e-mail: araki@mit.edu).

of integrated electronics are nowhere near as refined and user-friendly as those for creating mechanisms. For example, the fingers of the iRobot-Harvard-Yale (iHY) Hand [8], [9] integrate electronics by inserting a prefabricated circuit with wiring into a mold before epoxy is cast. In processes such as this, the electrical system is separately pre-fabricated, and care must be taken to ensure that components are placed properly within the mold throughout the entire fabrication process.

In this paper we describe a method of creating a three-dimensional circuit layout directly within the 3D printed part using hollow channels, Fig. 1c, and then depositing conductors directly into those by injecting a low-melting temperature metal that hardens when cool, as seen in Fig. 1b. Along with the fabrication process, we also describe a way to use existing circuit design tools, such as a typical board layout shown in Fig. 1a, to automatically generate the 3D CAD model of a part with the equivalent channels ready for injection. Prior to injecting the metal conductors, the surface of the part is populated with the discrete electronic components, which are then connected and held in place when the conductor hardens. Thus, the part made through the AM process serves as both the structural component of the robot and the printed circuit board. We demonstrate this concept within parts produced on a commercial FDM printer with subsequent injection of liquid metal into channels within the 3D printed parts, but the process is compatible with many commercial AM processes and does not require modification of the machine itself.

The remainder of this paper is broken into several sections. In Section II, an overview of available materials and techniques for rapid fabrication of circuits is presented, in conjunction with the available design parameters for liquid metal injection. Section III lays out the process parameters for liquid metal injection of circuits and the mechanics associated with the travel of liquid metal along channels during injection. Then, Section IV describes the tools and algorithms used to automatically generate the 3D model of the circuit from standard design tools. Section V discusses several experiments comparing the theory presented in Section III with experimental results, concluding with two example parts that demonstrate the features of the liquid metal injection technique. Section VI presents conclusions about this method of rapid prototyping circuits inside of traditional rapid-prototyped parts.

Related Work

The creation of circuits using AM processes is a rapidly evolving research area, and one in which the functional requirements vary significantly depending on the precise niche application. In this section we review both methods of printing conductive structures and materials as well as materials commonly used to create 3D printed circuits.

Conductive materials used for rapid prototyping circuits include slurries and composites, such as carbon nanofiber epoxies [10], carbon black composites [11], conductive silicone [12], conductive paints (such as Bare Paint [13]), and conductive inks like silver nanoparticle inks [14]. Each of these existing materials has its own set of challenges ranging from high cost and difficulty in fabrication, relatively high resistivity, and fabrication temperatures that preclude use with existing methods of additive manufacturing [15].

Other recent methods and materials include free-standing microstructures composed of liquid metal beads have been created using a 3D printer with a specialized extruder [16] and injecting room temperature liquid metal into already-formed structures [17]. Liquid traces such as these would be difficult to keep in place long term with an FDM part due to their porosity, though this work is a good example of high-conductivity, geometrically structured circuit traces, and significant parts have been adapted for the present work.

Early work on rapidly prototyped circuits consisted mostly of depositing capacitors or resistors directly onto printed circuit board [18]. Later, pioneering work in multi-material printing, where the secondary material was conductive silicone, was done by Periard, Malone, and Lipson [12]. This work allowed the circuit to be embedded within the 3D printed part. More recent work has developed a variety of methods for printing circuits on the surface of rapid-prototyped parts, using either conductive SLA materials or filling the channels as a post-print step [19]–[22]. This most recent work was limited to single layer circuits and utilize multiple interlocking parts or multiple faces of the part to implement more complex circuits that cannot be achieved with a single layer.

The work presented in this paper provides an alternative to the existing methods that has the added benefit in that it can (1) be used with existing single-material SLA and FDM printer through a post-print injection step, (2) accommodate multi-layer circuit designs, (3) can be embedded anywhere in the part with only the discrete component on the surface of the part, and (4) circuits can be generated using traditional circuit design tools and automatic conversion to the RP circuit is presented.

II. Process Overview

The process for creating injected metal circuits is diagrammed in Fig. 2. First, a series of small channels are designed into a solid part, and printed on a FDM printer. These channels are each connected to a single sprue (or injection point) used to fill the channel. Any electrical components making a connection with the channels are inserted through connected holes on the surface of the part. The injection apparatus consists of a syringe pump, syringe, reservoir of liquid metal, two check valves, tubing, and the industry standard slip tip tube fitting. The first bi-directional check valve allows the syringe in the pump to draw in liquid metal when retracting and to infuse liquid to the circuit when moving forward. The second check valve only allows forward pumping so as to keep the tubing primed with the liquid metal.

During infusion, the metal flows through the injection point, fills the channels until reaching the electrical connections at the surface. Traces harden when cooling upon removal from the heated enclosure and act as a solder holding inserted components in place to create electrical connections with component pins. Many of the process parameters must be carefully chosen to achieve successful injections. Material choice, trace sizing, and component insertion are all affected by a variety of other factors – for example, operating

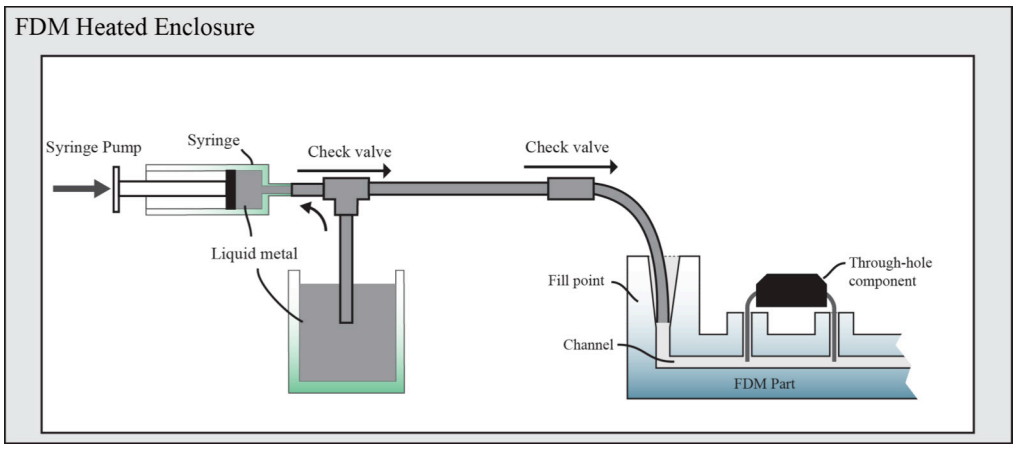

Figure 2. A schematic of the integrated wiring process, including the syringe pump, reservoirs, checks valves, and printed channels into which liquid metal is injected. Each trace within the part has a sprue, or injection point, used to fill the trace and the outlet of the injection device seals into the injection port using standard slip tip syringe connectors. The check valve ensures that the injection pathway remains primed with liquid metal between injections.

temperature, material properties, and printer settings. This section analyzes the most critical design parameters and provides guidelines that produce repeatable results.

A. Choice of Alloy

The choice of metal for wiring is heavily constrained by the thermal material properties of both the metal and the rapid-prototyped part, as well as the temperature at which injection takes place and the operating temperature of the circuit. The metal must be liquid at a temperature that the printed parts can withstand, but must also solidify at a high enough temperature to be reliably solid at room temperature and when running acceptable amounts of current through the solidified wires. The upper temperature bound was chosen based on the properties of ABS, the plastic most commonly used in FDM printers. This plastic never melts, but becomes soft at its glass transition temperature of 108 °C [23]. The lower bound of the desired metal melting point was chosen to be 50 °C, which is sufficiently far above room temperature that a wire carrying limited current should never melt. Most of the commercially available metals that melt in this range are not pure metals, but eutectics – alloys having the special property of melting at a single temperature rather than gradually melting over a range of temperatures. Of these eutectic mixtures, many are unsuitable because they include highly toxic metals, most notably cadmium.

We chose to use Cerrolow 136, a eutectic mixture of bismuth (49%), indium (21%), lead (18%) and tin (12%) [24]. This alloy melts at 57.8 °C and contains less lead than many of the alternative choices. Cerrolow 136 also has the desirable property of having almost no net volume change (0.0023% per degree Celsius) as it solidifies. This is useful because it does not have a tendency to warp and deform the parts as it cools, or to crack or bubble, creating breaks in the traces.

Cerrolow 136 has a resistivity of 7.081e-7 Ω-m, which is higher than copper (1.68e-8 Ω-m) but typical of many solders (~1.45e-7 Ω-m), and certainly much lower than many carbon-polymer composites [10]–[12]. A $0.8\times0.8\ mm^2$trace, equivalent in area to a 19 AWG copper wire, has approximately the same resistance per meter as copper wire between 35 and 36 AWG,

$$\frac{R}{L}=\frac{\rho}{A}=\frac{7.081e-7}{6.4e-7}=1.11\frac{\Omega}{m}, \quad (1)$$

where R is resistance, L is the length of the conductor, ρ is the conductivity of the Cerrelow 136, and A is the cross-sectional are of the conductor. Such a wire is rated by the National Fire Protection Association at between 0.21 and 0.27 Amperes continuous load [25], which is sufficient for supplying power to sensors, microprocessors and other discrete components, as well as power to small motors.

B. Trace Size and Spacing

The size of the traces used in the parts is partially governed by the size of the channels that can be printed into parts and partially governed by the properties of the liquid metal used. The minimum feature size on a commercial grade FDM printer is 0.36-0.63 mm, and it was experimentally determined on the authors' Fortus 250mc (Stratasys, MN, USA) that channels smaller than $0.8\times0.8\ mm^2$ exhibited occasional blockages due to unpredictable print irregularities and variability in actual dimension. For reliability, a minimum profile of $0.8\times0.8\ mm^2$ and a maximum profile of $1.6\times1.6\ mm^2$ were used throughout all experiments. Fig. 3 shows two different potential channel orientations with respect to the manner in which FDM layers are deposited. Most FDM printers allow a nominal amount of overhang before it requires support material to fill in the gap left by a void. At the larger $1.6\times1.6\ mm^2$ channel size, the square channel on the left in Fig. 3 would require support material. No support material would be required regardless of channel size for the diamond shaped channel shown on the right of Fig. 3. Channel geometries that would require support material are avoided and the diamond shape is used through all experiments.

The spacing between traces was bounded from below by the tendency of the liquid metal to leak between channels, and consequently create a short circuit, if the separation becomes too small. To avoid this, the circuit channels were spaced at twice the minimum feature size, so that two contours of solid ABS lay between them. When possible, four contours were used to further prevent leakage between channels. Fig. 4 depicts the spacing used, where yellow represents the deposited contours with two channels on either side.

C. Injection and Venting

Both the syringe full of liquid metal and the printed part must be fully above 57.8 °C in order to ensure that the injection process is reliable. Otherwise, the liquid metal can solidify midway through the infusion of a trace, causing a blockage and a failure to reach all components connected to the trace. In practice, this is accomplished by keeping both the syringe and the printed part in the heated enclosure of the 3D printer during injection. Most commercial printers hold their enclosures at 75 °C. If each outlet at a component pin is properly vented, a small amount of material should be visible at the completion of the injection process. If any blockage occurs during injection, whether due to solidification due to cooling or due to a print error, the possibility of leakage increases due to the semi-porous nature of fused deposition manufacturing and the increase in pressure may be sufficient to force the liquid metal through small features that would not appear porous at lower pressures.

When multiple traces branch out from a single injection point, it is crucial that the ends of each branch be properly vented to allow air to escape. This is usually accomplished by making sure that the holes in which components are inserted are loosely fit around the component pins or wires. It is also beneficial to avoid large differences in length between branches of the trace, as short branches may then overflow and leave long branches unfilled. The injection point may need to be judiciously placed to accomplish this. Section III presents models and simulations for injections including branching based on the volumetric flow rate down each branch and Section IV present an algorithm for determining the appropriate cross-sectional area of each channel segment to ensure that the advancing liquid metal reaches all of the vents and component pins simultaneously, thus eliminating spillage.

III. Injection Fluid Mechanics

One key objective for the liquid metal injection is to do a single injection for each portion of the circuit that has equivalent electrical potential (a "node voltage" in circuit terminology) such that the liquid metal reaches the outlet at the pins of the discrete components simultaneously. In order to achieve this goal, factors such the volumetric flow rate of the injected metal, the length and diameter of each channel, and the topology of the branching channels from injection to vent must be considered.

A simplified model for the advancing fluid is based on the Hagen-Poiseuille equation, which describes the relationship between the pressure drop in a fluid flowing through a cylindrical pipe,

$$\Delta P = \underbrace{\frac{128\mu L}{\pi d^4}}_{R} Q, \qquad (2)$$

where μ is the dynamic viscosity in Pa-s, d is the channel diameter in meters, L is the fluid length in meters, and Q is the volumetric flow rate in m^3/s. The entire term R can be thought of as the fluid flow resistance. That is, the pressure drop along the channel is function of the resistance to flow and the volumetric flow rate. The average fluid velocity can be computed from the volumetric flow rate as

$$V_{ave} = \frac{Q}{A} = \frac{4}{\pi d^2} Q. \qquad (3)$$

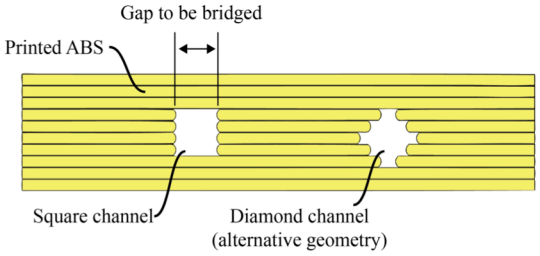

Figure 3. Channels for electrical traces were made using square profiles in the printed parts. To avoid printing support material into the traces, a diamond-shaped channel may be necessary.

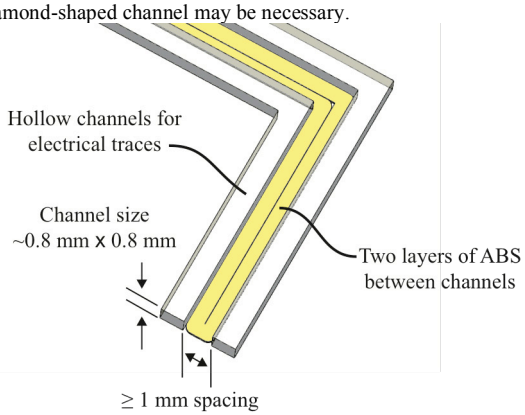

Figure 4. The channels must be spaced so that two widths of the printed ABS filament can fit between them.

For an advancing fluid head, the length of the liquid metal inside the channel is then a function of time, the fluid material properties, the channel geometry, and the volumetric flow rate,

$$L(t) = \int_0^t V_{ave} d\tau = V_{ave}\tau|_0^t = \frac{4}{\pi d^2} Qt. \qquad (4)$$

And, while the use of the Hagen-Poiseuille equation describes the flow of fluid in a single channel with advancing fluid, in the proposed method for RP circuit creation there are multiple branches of the channels and a model of fluid behavior must be derived for arbitrary branching.

Several simplifying assumptions are made to the model: (1) any oxidization and other effects that occur at the advancing fluid front that may cause the fluid advancement to not be accurately described by the Hagen-Poiseuille equation are neglected, (2) pressure drops that occur at branching junctions and at changes in the channel diameter are neglected, (3) the pressure drop between the advancing fluid and the outlet of the trace is neglected due to the fact that the pressure drop due to the ambient air is orders of magnitude less than the pressure drop in the fluid because of the difference in viscosity between the metal and the air, and (4) it is assumed that the syringe pump pushing liquid metal into the channels can exert sufficient force to keep the incoming volumetric flow rate constant regardless of the back pressure. These simplifications could be relaxed in future work, but they facilitate the channel diameter optimization described in the subsequent section, which ensures that the fluid reaches the component pins on the surface of the part almost simultaneously.

Using these assumptions, the relative volumetric flow rate down each of the channels at a branch point can be computed based on the resistance to fluid flow exhibited by

each of the channels. Fig. 5 shows the advancing fluid flow at two different points in time for a series of branching channels. In Fig. 5a, the fluid flow in each of the channel splitting from the main channel would be:

$$Q_2 = \frac{R_3}{R_2+R_3} Q_1 \text{ and } Q_3 = \frac{R_2}{R_2+R_3} Q_1. \quad (5)$$

In general, the flow down the k-th channel, Q_k can be computed as

$$Q_K = \frac{R_T}{R_K+R_T} Q_{in}, \quad (6)$$

where R_k is the fluid flow resistance of the k-th channel, R_T is the parallel equivalent fluid flow resistance of all other channel from the branch point, and Q_{in} is the volumetric flow rate coming into the branch point. Thus, as an example, the volumetric flow rate Q_3 in Fig. 5b would be

$$Q_3 = \frac{R_2 + R_4||R_5}{R_3+R_2+R_4||R_5} Q_1, \quad (7)$$

with parallel fluid flow resistance computed as

$$R_i||R_j = \frac{1}{\frac{1}{R_i}+\frac{1}{R_j}}. \quad (8)$$

Experiments comparing simulated fluid flow rates with those from actual injections is presented in Section V.

IV. Automating Circuit Generation

Traditionally, printed circuit boards are designed in specialized computer aided design (CAD) software. In software such as EAGLE PCB (CadSoft Inc., FL, USA) or OrCAD (Cadence Design Systems Inc., CA, USA), this is done as a three step process consisting of (1) schematic capture, (2) board layout, and (3) post-processing of board layout to generate layers, masks, and drill holes. To facilitate the generation of rapidly prototyped circuits using the principles and techniques described in Section II and Section III, an automated procedure to generate 3D printable parts with the embedded circuit in Standard Tessellation Language (STL) format was devised. This MATLAB (The Mathworks Inc., MA, USA) software took the output of step 2 above, a .BRD file from the EAGLE PCB, and generated the corresponding STL file representing the circuit.

A key challenge for injectable circuits is the desire to have the injected metal reach all the pins of a particular channel simultaneously. Not only will this limit spillage at the terminals of the electronic components, but will also prevent undesired shorts between components. This is achieved by algorithmically determining the appropriate channels diameters for each section along the injection path to either allow or restrict flow, thus achieving the objective.

The .BRD file format from EAGLE PCB is a human readable extensible markup language (XML) file. Using the XML parsing libraries provided by Matlab the circuit board was parsed into its key features, namely (1) injection points, (2) the starting and ending coordinates and layer of each segment of an electrical trace, (3) vias between layers, and (4) through-holes connecting all layers to the component location on the surface of the board. During the circuit board design process, an additional pin location was added to each of the traces in the circuit to act as the injection point. An example of each of these features is shown in Fig. 6.

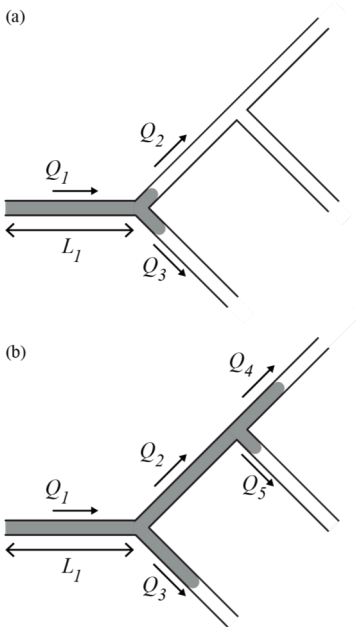

Figure 5. The advancing fluid flow with branching where the branching flow is determined by relative fluid flow resistance in each channel: (a) the first branch point has been reached and (b) multiple branches have occurred.

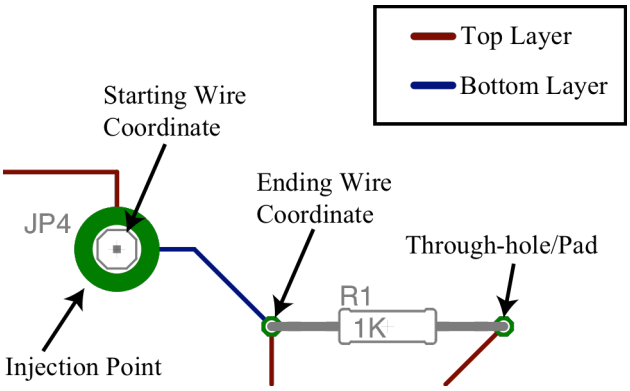

Figure 6. A diagram of the types of circuit elements that must be converted from the layered PCB format to an equivalent three-dimensional representation.

After a complete trace, or connected set of channels with equivalent electrical potential, was extracted from the .BRD file, Fig. 7a, the list of board features was organized into a tree structure beginning with the injection point and branching to reach each of the component pin locations, shown in Fig. 7b. The tree was then traversed, Fig. 7c, to generate a programmatic CAD representation of the circuit using the open-source OpenSCAD language (www.openscad.org) after which the OpenSCAD software generated an STL file, Fig. 7d, suitable for use in the authors' FDM printer.

The diameters of each of the segments of a particular trace is optimized such that the liquid metal reaches each component pin with the minimum variance in arrival time. Using the simplified fluid mechanics described in Section III and the parsed tree representation of a trace from injection to all of its component pin outlets, a simulation of the fluid flow including branching was implemented. The inputs to the simulation were the diameters and lengths of each segment within the trace, a simulation time step, the volumetric flow

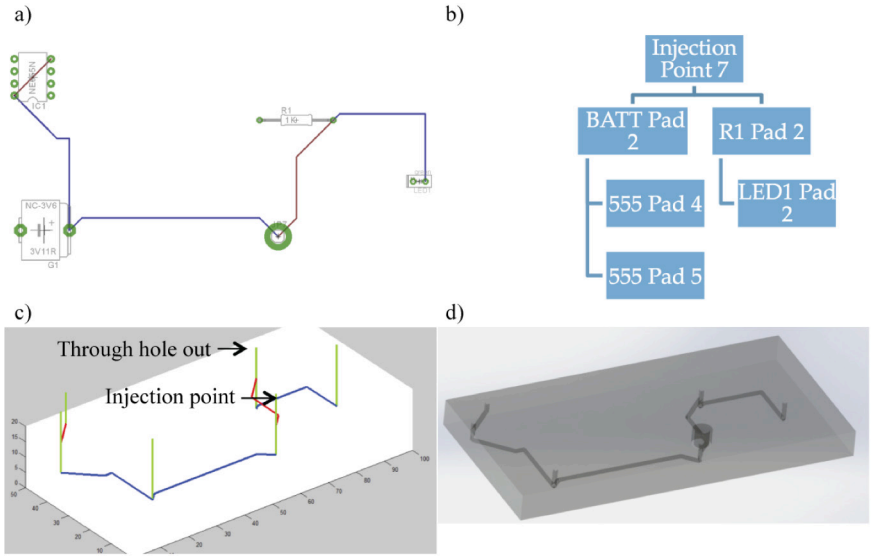

Figure 7. The complete process of conversion of a single trace from circuit board CAD software (EAGLE PCB) to the equivalent 3D printed part with channels ready for injection: (a) The EAGLE PCB representation of a single trace of the circuit, (b) the extracted tree representation of the trace starting at the injection point and ending at each component pin location, (c) a plot of the extracted tree with layer depths and channel diameters specified, and (d) the conversion of the circuit trace tree representation to STL format using the programmatic solid modeling language and software OpenSCAD.

rate from the injection device, and the topology of the trace from injection to outlets. The output of this simulation was a set of times $\{t_k\}$ representing the times at which the fluid would begin exiting each component pin outlet hole. Then, a constrained optimization was executed, where the circuit topology was fixed and the optimization was over the channel diameters, d_p. The optimization constraints were a minimum channel cross-sectional area of $0.8{\times}0.8\ mm^2$ and a maximum cross-sectional area of $1.6{\times}1.6\ mm^2$, with the optimization criterion being the minimization of the variance of $\{t_k\}$.

$$\{d_p^*\} = \underset{\{d_p\}}{\operatorname{argmin}}\, var(\{t_k\}), 0.8\ mm < d_p < 1.6\ mm. \quad (9)$$

The algorithm for simulating a single injection is available upon request from the corresponding author. This minimization ensured that we found a local minimum where the time at which the metal reached the component pin outlet holes was small.

V. Design Experiments

A variety of design experiments were conducted to validate the proposed method of printing channels into 3D printed parts with subsequent injection of liquid metal. The experiments explored a variety of expected outcomes for repeatability and quality including: (1) the effects of branching and varying channel diameters along the branches, and (2) creating a mobile robot body and circuit using discrete components and the circuit generation algorithm described in Section IV.

A. Branching Channels

To explore the effects of channel diameter on the travel of liquid metal through circuits, a branching test piece, shown in Fig. 8a was created. The advancing head of the liquid metal was tracked in each channel by capturing video of the part during injection and performing background image subtraction to accentuate the visible difference between an empty and full channel. An example trial at three different time intervals during a single insertion is shown in Fig. 10b-d.

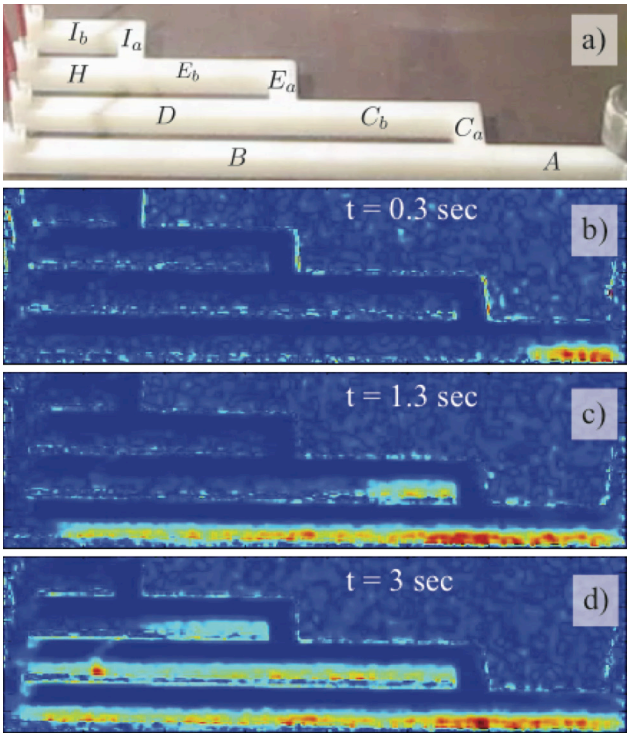

Figure 8. The branching test piece and visual tracking of fluid advancement through background image subtraction using a visible light camera: (a) the branching test piece where the diameter of the channels in each of the four branches can be varied and (b)-(d) the advancing liquid metal for a single injection at three different times.

The visible-light camera technique used to track the advancing head of the fluid in each channel can only detect fluid flow in the channels aligned horizontal to the camera because it relies on light passing through the thin ABS parts to distinguish between an empty and full channel. So, when

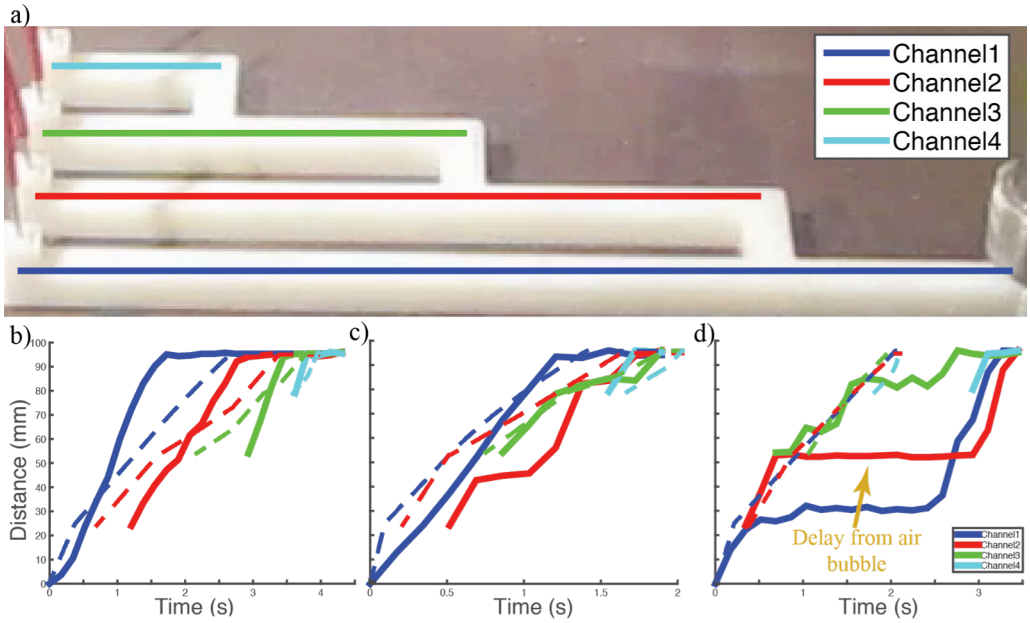

Figure 9. Injection simulations (dashed lines) and experimental results (solid lines) including potential error conditions: (a) the branching test piece used to compare injection simulations with experimental results, (b) all channels are 0.8 x 0.8 mm^2, (c) the first channel is 0.8 x0.8 mm^2 and each successive channel has 2-,3-, and 4-times the cross sectional area, and (d) the optimized channel diameters. Note that in the case of the optimized channel diameters that a bubble in the injection pathway caused a delay during injection, but that the variance in final arrival time was less than the non-optimized cases despite the delay. Because the visual fluid tracking only allowed us to track fluid in the horizontal direction, only the position of the fluid head in each horizontal channel is plotted.

comparing the simulated and experimental results, we only track the position of the fluid head in each channel as indicated in Fig. 9a.

The simulated and actual injections were compared for three different kinds of channel diameters: (1) constant for all channels, (2) increasing for each successive channel, and (3) optimized based on the simulations using the algorithm from Section IV. Fig. 9b shows the simulation (dashed lines) and experimental result (solid lines) for the branching test piece where all channels were $1.6\times1.6\,mm^2$ in cross-sectional area. The fact that the earlier branches fill more quickly than the simulation suggests may indicate that the pressure drops due to branching, turns, and diameter changes should be incorporated into the simulation. Fig. 9c shows simulation results where the smallest channel has a cross-sectional area of $A=0.8\times0.8\,mm^2$ and each successive channel has a cross sectional area of 2A, 3A, and 4A, respectively. Finally, the branching test piece with optimized channel diameters is shown in Fig. 9d (d=[1.177, 0.970, 1.474, 1.474, 0.919, 1.348, 1.348, 1.199, 1.168, 1.168] *mm*, where the segment definitions are given in Fig. 8a as segments A through I_b). This trial, despite experiencing a delay due to a bubble during injection, indicates that optimizing the channel diameters is able to effectively ensure that all channels reach their outlets with the minimum variance in arrival time, compared to the nominal (not optimized) diameters.

B. Differential-drive Robot

The final, more difficult demonstration part was an entire differential-drive robot, depicted in Fig. 1. This robot was printed as a part including the mounting holes for the gear motors, the solid caster, and the circuit near the top surface of the 3D printed part. The circuit consisted of an Arduino Micro, two full H-Bridges (Toshiba TA7291), and headers for power from a battery and to the motors. The part count was low enough to be implemented with a simple two-layer board, yet complicated enough to be a non-trivial demonstration. The circuit was first designed in EAGLE PCB using standard schematic capture (Fig. 1a) where the only additional circuit component that would not normally be included in a schematic design are the isolated pins representing the injection points. This schematic was used to generate a board layout (Fig. 1b), and the autorouting constraints were modified for a minimum of 80mil trace-to-trace distance to ensure the minimum number of contours could be achieved in the FDM printed part. The resulting .BRD file from the board layout process was parsed, the channel sizes optimized, and the 3D printed part was generated in STL format. All of the metal traces were injected into a block of printed ABS, and each trace contained multiple holes for the insertion of component leads.

The population of the circuit, shown in Fig. 1c, was done as part of the injection process where the components were already in place while injecting the liquid Cerrelow 136. After all injections were completed, there was a error where a single pin on each H-Bridge chip had not made a connection (Pin6 of the TA7291 for both ICs). This was corrected by injecting again and allowing more spillage out the other connected holes to ensure the connection at the problematic pins had been made. Any spillage was cleaned

from the surface through light scraping after the part was removed from the heated enclosure and the metal had cooled.

The robot worked as expected and continuous driving showed that the minimal amount of current draw by these motors, approximately 0.1A during normal operation, was low enough to prevent the traces from heating and melting from Joule heating.

VI. Conclusion

The goal of this work was the development and dissemination of methods for improving the performance of rapidly prototyped robots. The automated method presented here uses traditional circuit prototyping techniques and translates the results into 3D model appropriate for printing using rapid prototyping methods. As one of the revolutionary aspect of additive manufacturing is the ability to create structures and components that cannot be manufactured using traditional fabrications techniques, RP circuits also have the potential to be transformative in allowing sensing, actuation, and other electronics to be seamlessly incorporated into mechanical components. This particular approach is much less time-consuming than manually wiring and inserting a large number of sensors into a rapidly prototyped device and has the advantage over many other existing RP circuit techniques in that is allows intrinsically multi-layered designs. Considering the benefits reaped so far by experimental roboticists from rapid prototyping technology, the development of integrated rapid prototyped circuits is a logical next step. This paper has shown that liquid metal injection is feasible, and has described a set of process parameters that enable anyone with a FDM printer to make printed ABS circuits using existing circuit design tools.

Acknowledgment

The authors thank Alejandro Carrillo, Gerardo Carranza, and Tom Bu for their assistance in process development, testing, and experiment hardware.

References

[1] R. Merz, F. B. Prinz, K. Ramaswami, M. Terk, and L. Weiss, *Shape deposition manufacturing*. Engineering Design Research Center, Carnegie Mellon Univ., 1994.

[2] T. Laliberte, C. M. Gosselin, and G. Cote, "Practical prototyping," *IEEE Robot. Autom. Mag.*, vol. 8, no. 3, pp. 43–52, 2001.

[3] M. Quigley, A. Asbeck, and A. Ng, "A low-cost compliant 7-DOF robotic manipulator," in *2011 IEEE International Conference on Robotics and Automation*, 2011, pp. 6051–6058.

[4] R. R. Ma, L. U. Odhner, and A. M. Dollar, "A modular, open-source 3D printed underactuated hand," in *2013 IEEE International Conference on Robotics and Automation*, 2013, pp. 2737–2743.

[5] E. Malone and H. Lipson, "Fab@Home: the personal desktop fabricator kit," *Rapid Prototyp. J.*, vol. 13, no. 4, pp. 245–255, 2007.

[6] J. G. Cham, S. A. Bailey, J. E. Clark, R. J. Full, and M. R. Cutkosky, "Fast and Robust: Hexapedal Robots via Shape Deposition Manufacturing," *Int. J. Rob. Res.*, vol. 21, no. 10–11, pp. 869–882, Oct. 2002.

[7] A. M. Dollar, C. R. Wagner, and R. D. Howe, "Embedded Sensors for Biomimetic Robotics via Shape Deposition Manufacturing," in *Biomedical Robotics and Biomechatronics, 2006. BioRob 2006. The First IEEE/RAS-EMBS International Conference on*, 2006, pp. 763–768.

[8] L. U. Odhner, L. P. Jentoft, M. R. Claffee, N. Corson, Y. Tenzer, R. R. Ma, M. Buehler, R. Kohout, R. D. Howe, and A. M. Dollar, "A compliant, underactuated hand for robust manipulation," *Int. J. Rob. Res.*, vol. 33, no. 5, pp. 736–752, Feb. 2014.

[9] Y. Tenzer, L. P. Jentoft, and R. D. Howe, "Inexpensive and easily customized tactile array sensors using MEMS barometers chips," *IEEE Robot. Autom. Mag. (In Press.*, 2014.

[10] J. Czyżewski, P. Burzyński, K. Gaweł, and J. Meisner, "Rapid prototyping of electrically conductive components using 3D printing technology," *J. Mater. Process. Technol.*, vol. 209, no. 12–13, pp. 5281–5285, Jul. 2009.

[11] S. J. Leigh, R. J. Bradley, C. P. Purssell, D. R. Billson, and D. A. Hutchins, "A simple, low-cost conductive composite material for 3D printing of electronic sensors.," *PLoS One*, vol. 7, no. 11, p. e49365, Jan. 2012.

[12] D. Periard, E. Malone, and H. Lipson, "Printing embedded circuits," in *Proceedings of the 18th Solid Freeform Fabrication Symposium, Austin TX*, 2007, pp. 503–512.

[13] "Bare Paint Technical Data Sheet," *Bare Conductive*, 2013. [Online]. Available: http://www.bareconductive.com/wp-content/uploads/2013/11/2013.TechnicalDataSheet_ElectricPaint.pdf. [Accessed: 07-Feb-2014].

[14] Y. Kawahara, S. Hodges, B. S. Cook, C. Zhang, and G. D. Abowd, "Instant Inkjet Circuits: Lab-based Inkjet Printing to Support Rapid Prototyping of UbiComp Devices," in *Proceedings of the 2013 ACM International Joint Conference on Pervasive and Ubiquitous Computing*, 2013, pp. 363–372.

[15] T. H. J. van Osch, J. Perelaer, A. W. M. de Laat, and U. S. Schubert, "Inkjet Printing of Narrow Conductive Tracks on Untreated Polymeric Substrates," *Adv. Mater.*, vol. 20, no. 2, pp. 343–345, 2008.

[16] C. Ladd, J.-H. So, J. Muth, and M. D. Dickey, "3D printing of free standing liquid metal microstructures.," *Adv. Mater.*, vol. 25, no. 36, pp. 5081–5, Sep. 2013.

[17] A. Fassler and C. Majidi, "3D structures of liquid-phase GaIn alloy embedded in PDMS with freeze casting.," *Lab Chip*, vol. 13, no. 22, pp. 4442–50, Nov. 2013.

[18] W. Jillek and W. K. C. Yung, "Embedded components in printed circuit boards: a processing technology review," *Int. J. Adv. Manuf. Technol.*, vol. 25, no. 3–4, pp. 350–360, Jul. 2004.

[19] D. Espalin, D. W. Muse, E. MacDonald, and R. B. Wicker, "3D Printing multifunctionality: structures with electronics," *Int. J. Adv. Manuf. Technol.*, vol. 72, no. 5–8, pp. 963–978, Mar. 2014.

[20] E. Macdonald, R. Salas, D. Espalin, M. Perez, E. Aguilera, D. Muse, and R. B. Wicker, "3D Printing for the Rapid Prototyping of Structural Electronics," *IEEE Access*, vol. 2, pp. 234–242, Dec. 2014.

[21] A. Joe Lopes, E. MacDonald, and R. B. Wicker, "Integrating stereolithography and direct print technologies for 3D structural electronics fabrication," *Rapid Prototyp. J.*, vol. 18, no. 2, pp. 129–143, 2012.

[22] E. DeNava, M. Navarrete, A. Lopes, M. Alawneh, M. Contreras, D. Muse, S. Castillo, E. MacDonald, and R. Wicker, "Three-dimensional off-axis component placement and routing for electronics integration using solid freeform fabrication," in *Proceedings of Solid Freeform Fabrication Symposium, The University of Texas at Austin, Austin TX*, 2008, pp. 362–369.

[23] "ABSplusTM-P430 Technical Data Sheet," *Stratasys, Ltd.*, 2013. [Online]. Available: http://www.stratasys.com/~/media/Main/Secure/Material Specs MS/Fortus-Material-Specs/Fortus-MS-ABSplus-01-13-web.ashx. [Accessed: 07-Feb-2014].

[24] "Bolton Metals Specifications," *Bolton Metal Products Company*, 2013. [Online]. Available: http://www.boltonmetalproducts.com/Specifications.html. [Accessed: 07-Feb-2014].

[25] *National Electrical Code 2008*. National Fire Protection Association, 2007.

[26] Q. Xu, N. Oudalov, Q. Guo, H. M. Jaeger, and E. Brown, "Effect of oxidation on the mechanical properties of liquid gallium and eutectic gallium-indium," *Phys. Fluids*, vol. 24, no. 6, p. 063101, Jun. 2012.